OPTIMIZING INTEGRATED-OPTICS POLARIZERS FOR MAXIMUM POLARIZATION ISOLATION

Fernando J. S. Moreira*
Aluizio Prata, Jr.
University of Southern California
Los Angeles, CA 90089-0271, USA

Abstract

Available technologies currently permit the construction of optical integrated polarizers employing accurate features with dimensions considerably smaller than the operation wavelength. These devices may have a relatively small number of grooves and rely on the wave-polarization dependence of the groove scattering to achieve their results. To achieve optimum performance (e.g., maximum polarization isolation) they must be modeled with an accuracy only possible through the use of rigorous vector diffraction theory. In this work one such technique is applied to analyze and design perfectly conducting polarizers with finite number of arbitrarily-shaped features. The currents flowing on the grooves' surfaces are rigorously obtained, and from them the scattered field is determined. As an application example, the dimensions of the first and last grooves of a 20-triangular-grooves polarizer, operating at 1 μm wavelength, are optimized to yield a polarization isolation of 57 dB.

1. Introduction

Metallic gratings are widely used in a variety of optical applications such as spectroscopy, filters, diffractive-optics devices, and holography. Currently available technologies permit the construction of metallic (or dielectric) gratings with extremely small features, suitable for high-speed integrated optics operating at optical frequencies and beyond. Also, very accurate blazes are possible, permitting the construction of gratings with high diffraction efficiency operating at small wavelengths. It is now possible to control the shape of the grooves individually and accurately by using submicron integrated circuit technology, and hence small high-performance polarizers can be constructed. In order to design such polarizers the optimal shape of the grooves must be determined accurately, and for this task one needs the accurate modeling tools that can only be provided by rigorous vector diffraction theory [1].

In the past, several authors have dealt with the analysis of optical metallic gratings using vector diffraction theory [1], although in most cases only infinite periodic structures have been considered. Due to this, and to the efforts of the antenna and microwave communities, several techniques are currently available to rigorously handle optical polarizers. In the present work the Electric and Magnetic Field Integral Equations [2],[3] have been selected to tackle the problem. They are relatively easy to implement, yield very accurate results, and can handle arbitrarily-shaped metallic grooves. The polarizers considered here are assumed to be made of a perfectly conducting material and to have a finite number of infinitely-long grooves. Two-dimensional integral equations are used to determine the scattered fields exactly (in a numerical sense), and to optimize the polarizer for maximum polarization isolation. The formulation presented assumes an arbitrary plane-wave illumination and can be readily extended to polarizers operating under more complex illuminations (e.g., Gaussian beams).

0-7803-2674-1/95/$4.00 © 1995 IEEE.

2. Rigorous Analysis of Grating-Type Polarizers

The objective of this section is to briefly outline the formulation necessary for the numerical determination of the electromagnetic fields scattered by a perfectly-conducting grating-type polarizer. The grating is assumed to have a finite number of arbitrarily-shaped infinitely-long grooves and is illuminated by an arbitrarily-polarized uniform plane wave (see Fig. 1). Although in the examples to be shown the wavenumber vector $\vec{k}$ is assumed in the $z = 0$ plane, the formulation can in principle handle a plane-wave illumination with an arbitrarily oriented $\vec{k}$. The grating geometry is independent of the z coordinate, permitting the application of a two-dimensional vector scattering formulation based on the Electric and Magnetic Field Integral Equations (EFIE and MFIE, respectively) [2].

For an arbitrarily oriented vector $\vec{k}$, α is the angle that $\vec{k}$ makes with the $\hat{z}$ direction. Although the grating geometry does not depend on z, an incident plane wave with $\alpha \neq 90°$ will introduce a z-dependence factor of the form $\exp(-jkz\cos\alpha)$ in the formulation, where $k = |\vec{k}| = 2\pi/\lambda$ and λ is the wavelength. Since this factor is present in all fields and currents, for simplicity it has been omitted throughout this work. A time-harmonic dependence is assumed and the corresponding factor $\exp(+j\omega t)$ (where ω is 2π times the wave frequency) has also been omitted from the following equations.

The incident plane wave can be decomposed into its corresponding TM- and TE-polarized counterparts (no magnetic $\vec{H}$ and electric $\vec{E}$ fields along the $\hat{z}$ direction, respectively). Note that, in optical theory, usually TM (TE) is defined for the polarization with electric (magnetic) field parallel to the plane of incidence. However, as the vector $\vec{k}$ orientation is considered arbitrary in the present work, this notation has been conveniently modified. For the TM polarization the EFIE is used, which can be written as [2]

$$E_z^{in}(\vec{\rho}) = \frac{\xi\eta\sin\alpha}{4}\int_C J_z(\vec{\rho}')\ H_0^{(2)}(\xi\,|\vec{\rho}-\vec{\rho}'|)\ dl', \tag{1}$$

where C is the grating cross-section contour (in the $z = 0$ plane), $E_z^{in}(\vec{\rho})$ is the $\hat{z}$-component of the incident electric field at an arbitrary point $\vec{\rho}$ located on the contour C, $J_z(\vec{\rho}')$ is the $\hat{z}$-component of the electric current density flowing at the point $\vec{\rho}'$ (also located at the contour C), $\xi = k\sin\alpha$, η is the free-space wave impedance ($\eta = 376.73031\,\Omega$), and $H_0^{(2)}$ is the zero-th order Hankel function of the second kind. For the TE polarization it is more convenient to use the MFIE [2]

$$H_z^{in}(\vec{\rho}) = \frac{H_z(\vec{\rho})}{2} + \frac{j\xi}{4}\int_C H_z(\vec{\rho}')\ H_1^{(2)}(\xi\,|\vec{\rho}-\vec{\rho}'|)\ \frac{(\vec{\rho}-\vec{\rho}')}{|\vec{\rho}-\vec{\rho}'|}\cdot\hat{n}\ dl', \tag{2}$$

where $H_z^{in}(\vec{\rho})$ is the $\hat{z}$-component of the incident magnetic field on the contour C, $H_z(\vec{\rho})$ is the $\hat{z}$-component of the total magnetic field (incident + scattered) immediately above the contour C, $\hat{n}$ is the outward pointing unit normal to the contour C, and $H_1^{(2)}$ is the first order Hankel function of the second kind. The integrands of Eqs. 1 and 2 have a removable singularity whenever $\vec{\rho} = \vec{\rho}'$, and the contour integration should be performed in a Cauchy principal value sense (as indicated by the notation used).

The unknowns in Eqs. 1 and 2 are the complex quantities $J_z(\vec{\rho}')$ and $H_z(\vec{\rho}')$. In the present work they are obtained by solving the above integral equations using the Method-of-Moments (plus Point-Matching) technique [3]. In this approach, the unknowns J_z and H_z are expanded

into a suitable set of basis functions over the contour C. Then Eqs. 1 and 2 are transformed into a linear system of equations that, once solved, give the coefficients of the basis-function expansions. Once $J_z(\vec{\rho}')$ and $H_z(\vec{\rho}')$ are determined, the $\hat{z}$-component of the scattered fields can be obtained using

$$E_z^S(\vec{\rho}) = \frac{-\xi\eta \sin\alpha}{4} \int_C J_z(\vec{\rho}')\ H_0^{(2)}(\xi\,|\vec{\rho}-\vec{\rho}'|)\ dl', \quad \text{for TM, and} \tag{3}$$

$$H_z^S(\vec{\rho}) = \frac{-j\,\xi}{4} \int_C H_z(\vec{\rho}')\ H_1^{(2)}(\xi\,|\vec{\rho}-\vec{\rho}'|)\ \frac{(\vec{\rho}-\vec{\rho}')}{|\vec{\rho}-\vec{\rho}'|}\cdot\hat{n}\ dl', \quad \text{for TE,} \tag{4}$$

where $\vec{\rho}$ now locates the observation point (still in the $z = 0$ plane accordingly to Fig. 1) and the superscript S stands for the scattered field, which is the total field minus the incident plane-wave one. For observation points with ρ much larger than the grating cross-section dimensions, the integrand of Eqs. 3 and 4 can be simplified to yield, for the TM polarization,

$$E_z^S(\vec{\rho}) = \frac{-\xi\eta \sin\alpha}{4}\sqrt{\frac{2}{\pi}}\ e^{j\pi/4}\ \frac{e^{-j\xi\rho}}{\sqrt{\xi\rho}} \int_C J_z(\vec{\rho}')\ e^{j\xi\,\vec{\rho}'\cdot\hat{\rho}}\ dl', \tag{5}$$

$$E_\rho^S(\vec{\rho}) = -\tan\alpha\ E_z^S(\vec{\rho}), \tag{6}$$

$$H_\phi^S(\vec{\rho}) = \frac{-1}{\eta\sin\alpha}\ E_z^S(\vec{\rho}), \tag{7}$$

$$E_\phi^S(\vec{\rho}) = H_\rho^S(\vec{\rho}) = H_z^S(\vec{\rho}) = 0, \tag{8}$$

and for the TE polarization,

$$H_z^S(\vec{\rho}) = \frac{\xi}{4}\sqrt{\frac{2}{\pi}}\ e^{j\pi/4}\ \frac{e^{-j\xi\rho}}{\sqrt{\xi\rho}} \int_C H_z(\vec{\rho}')\ e^{j\xi\,\vec{\rho}'\cdot\hat{\rho}}\ \hat{\rho}\cdot\hat{n}\ dl', \tag{9}$$

$$H_\rho^S(\vec{\rho}) = -\tan\alpha\ H_z^S(\vec{\rho}), \tag{10}$$

$$E_\phi^S(\vec{\rho}) = \frac{\eta}{\sin\alpha}\ H_z^S(\vec{\rho}), \tag{11}$$

$$E_\rho^S(\vec{\rho}) = E_z^S(\vec{\rho}) = H_\phi^S(\vec{\rho}) = 0. \tag{12}$$

The scattered power densities for the TM and TE polarizations can be obtained from Eqs. 5–12 and are given respectively by:

$$S^{TM}(\vec{\rho}) = \frac{1}{2\eta}\,|\vec{E}^S|^2 = \frac{1}{2\eta}\,\frac{|E_z^S(\vec{\rho})|^2}{\sin^2\alpha}, \tag{13}$$

$$S^{TE}(\vec{\rho}) = \frac{\eta}{2}\,|\vec{H}^S|^2 = \frac{\eta}{2}\,\frac{|H_z^S(\vec{\rho})|^2}{\sin^2\alpha}. \tag{14}$$

3. Polarizer Case Study

In this section, the previously presented formulation is applied to the design of perfectly-conducting grating-type polarizer. As a case study, the design of a polarizer composed of a finite number of infinitely-long triangular grooves is considered (see Fig. 1). Its initial geometry has been obtained assuming an infinite number of grooves, and requiring that only the TM (TE) polarization is present at its specular-reflection (backscattering) order. The design objective is to increase the isolation between the TM and TE polarizations at the specular reflection, which deteriorates when the infinite grating is truncated into a finite number of grooves. For the infinite grating, this polarization isolation can in principle be infinite.

The grating geometry was selected to have only two diffraction orders: one at $\phi = 30°$ (specular reflection) and the other at $\phi = 150°$ (backscattering direction). These directions were chosen in order to have a large angular separation between the two diffraction orders (120° for the present case). The incident plane wave has a operation wavelength λ of 1 μm and a 1 Volt/m electric-field amplitude. It has equal amounts of TM and TE polarizations and its wavenumber vector $\vec{k}$ lies in the $z = 0$ plane ($\alpha = 90°$), such that the incident angle θ_i is 60° (see Fig. 1). The grating period X_p to produce the above mentioned diffraction orders is given by [4]

$$\cos\phi_\ell = \ell\frac{\lambda}{X_p} + \sin\theta_i\,, \tag{15}$$

where ℓ is an integer number corresponding to the grating diffraction orders. In the present case, $\ell = 0$ and -1 correspond to $\phi_\ell = 30°$ and 150°, respectively, yielding $X_p = 0.57735$ μm. The desired polarization-isolation behavior can be achieved with the triangular profile shown in Fig. 1 (where $X_p = a + b$), provided that the incident wavenumber vector $\vec{k}$ is parallel to one of the groove walls and perpendicular to the other [1].

The above groove geometry has been used in the 20-triangular-grooves polarizer shown in Fig. 1. The scattered power densities, computed using the formulation presented in Sect. 2, are depicted in Fig. 2, where the power-density values have been conveniently normalized using

$$\tilde{S} = S \times \xi\rho, \tag{16}$$

where S is given by Eqs. 13 and 14. To ensure the numerical convergence of the Method of Moments, the grating contour C was divided into 0.03 segments/λ, as explained in Sect. 2. The normalized scattered power densities at $\phi = 30°$ are -6.01 dB and -43.34 dB for the TM and TE polarizations, respectively, yielding a polarization isolation of approximately 37 dB. Compared to the scattering produced by a flat metallic plate with the same dimensions, the polarizer diffraction efficiencies at $\phi = 30°$ are 90.2% (-0.45 dB) and 0.016% (-37.87 dB) for the TM and TE polarizations, respectively.

From the theory of diffraction gratings it is known that the scattered field amplitude, in a given direction ϕ, is related to both the existence of a diffraction order and to the particular grating-period geometry (i.e., its induced surface currents) [1]. This explains the small scattered field of the TE polarization at $\phi = 30°$ (see Fig. 2). Although a diffraction peak is expected, since the radiation of each grating period adds coherently towards this direction, this effect is cancelled by the small radiation of the currents towards the same direction. For the above polarizer geometry with an infinite number of grooves, the induced surface currents of the TE polarization radiate zero power density towards the $\phi = 30°$ direction. The finite 37 dB polarization isolation

observed in Fig. 2 is then caused by the finite length of the polarizer, which perturbs the ideal surface current distribution, specially near the polarizer edges. It can then be expected that the optimization of the groove shapes may correct this problem.

To test the above possibility, a numerical optimization of the groove shapes was performed in the 20-grooves polarizer. Considering the small TE scattered power level at $\phi = 30°$, only the shape of two grooves were adjusted. Since most of the current perturbation occurs in the grooves at the polarizer edges (1 and 20 in Fig. 1), these two grooves were optimized to increase the polarization isolation at $\phi = 30°$, while maintaining the TM scattered power level. Based on the parameters of Fig. 1, the dimensions given by the optimization procedure are $h_1 = 0.318\ \mu$m, $a_1 = 0.15735\ \mu$m, and $b_1 = 0.42\ \mu$m for groove 1, and $h_{20} = 0.229\ \mu$m, $a_{20} = 0.20235\ \mu$m, and $b_{20} = 0.375\ \mu$m for groove 20. The corresponding polarizer performance is shown in Fig. 3. This figure indicates that the normalized scattered power density peaks, at $\phi = 30°$, are -6.03 dB and -63.16 dB for the TM and TE polarizations, respectively. The polarization isolation has increased to 57 dB, a value 20 dB higher than the one of the non-optimized polarizer. The polarizer diffraction efficiencies, at $\phi = 30°$, are now 89.7% (-0.47 dB) and 0.0002% (-57.69 dB) for the TM and TE polarizations, respectively. It is interesting to note that the increased polarization isolation was obtained with a negligible cost to the diffraction efficiency of the TM polarization, which was reduced by only 0.5%.

Its important to observe that the above polarization-isolation improvement was obtained through cancelation effects. In other words, the first and last grooves were shaped so that the TE-polarized electromagnetic fields radiated by their corresponding surface currents (at $\phi = 30°$) partially cancel the undesirable fields produced by the currents of the remaining grooves. As a consequence, it can be expected that the polarizer improved isolation is relatively narrow band. This expectation is corroborated by the results of Fig. 4, which depict the polarization isolation dependence with the operation wavelength. However, this is a minor problem for most laser applications.

4. Conclusions

In this work the theory required to rigorously analyze and synthesize integrated-optics grating-type polarizers was presented. This vector diffraction theory is based on the Electric and Magnetic Field Integral Equations, which were applied to the design of a perfectly-conducting polarizer with a finite number of infinitely-long grooves. The formulation presented is capable of handling a completely arbitrary plane-wave illumination, making it readily extendable to more complicated field illuminations (e.g., Gaussian beams).

As an example of polarizer design, a perfectly-conducting structure with 20 triangular grooves was considered. The geometry was initially designed assuming an infinite number of grooves, which were subsequently truncated and analyzed. This polarizer yielded 37 dB of polarization isolation, combined with a diffraction efficiency of 90.2% for the TM polarization. This initial design was then optimized for maximum polarization isolation, by adjusting the shapes of the grooves at the polarizer edges. Through this, a polarization isolation of 57 dB was obtained with a negligible loss of the TM diffraction efficiency. This case study demonstrates the level of performance that can be expected from integrated-optics polarizers designed using accurate vector diffraction theory.

References

[1] R. Petit (editor), *Electromagnetic Theory of Gratings*, Springer-Verlag, Berlin, 1980.

[2] R. Mittra (editor), *Computer Techniques for Electromagnetics*, Taylor & Francis, Bristol, 1987, Ch. 4.

[3] R. F. Harrington, *Field Computation by Moment Methods*, IEEE Press, New York, 1993.

[4] M. Born and E. Wolf, *Principles of Optics*, 6th ed., Pergamon, London, 1980.

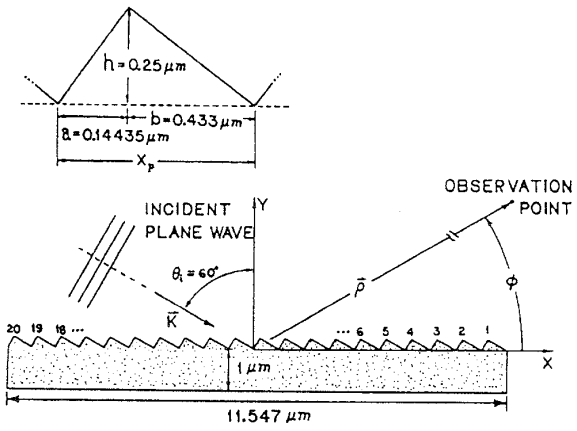

Fig. 1 – 20-grooves polarizer.

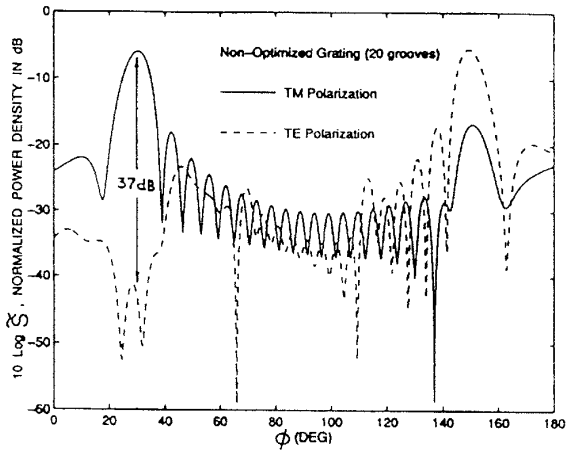

Fig. 2 – Non-optimized polarizer scattering.

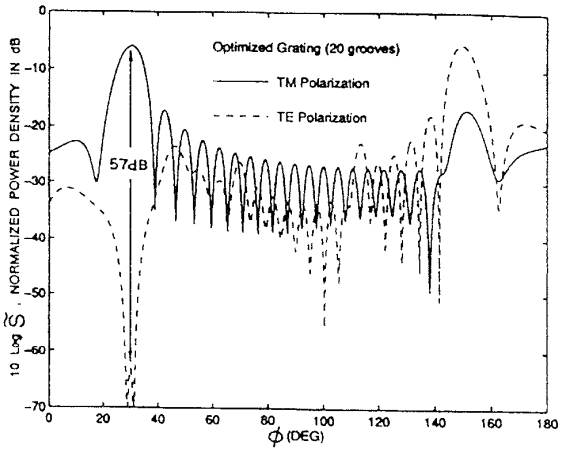

Fig. 3 – Optimized polarizer scattering.

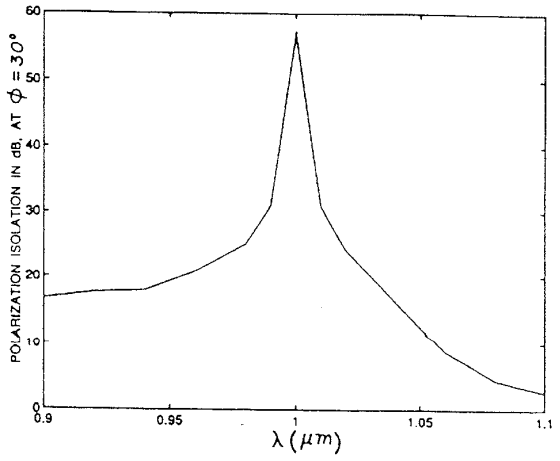

Fig. 4 – Optimized polarizer isolation.